COMPDYN 2015
5th ECCOMAS Thematic Conference on
Computational Methods in Structural Dynamics and Earthquake Engineering
M. Papadrakakis, V. Papadopoulos, V. Plevris (eds.)
Crete Island, Greece, 25–27 May 2015

A NEW SEISMIC DESIGN METHOD FOR DEEPLY EMBEDDED FOUNDATIONS ACCOUNTING FOR SSI EFFECTS

Nikos Gerolymos[1], and Athanasios Zafeirakos[2]

[1] National Technical University of Athens, Greece
9, Heroon Polytechniou Str., Polytechnic Campus, Zografos P.C 15780
e-mail: gerolymos@gmail.com

[2] National Technical University of Athens, Greece
9, Heroon Polytechniou Str., Polytechnic Campus, Zografos P.C 15780
e-mail: azafeirakos@gmail.com

Keywords: Deeply embedded foundations, seismic design, Soil structure interaction, Bearing strength surface, Material and geometrical nonlinearities.

Abstract. *A Seismic capacity design method for deeply embedded (or caisson) foundations is proposed based on 3D finite element analysis results. Emphasis is given on the influence of: (a) the kinematic constraints imposed by the superstructure, and (b) the nonlinear behaviour (due to both material and interface nonlinearities) of the foundation on the response of the SSI system. The method involves an analytical formulation of the load path at the caisson head level until complete failure. Interestingly, all load-paths display a particular "over-strength" in bearing capacity that is mobilized by the foundation, identified as the "inverted" pendulum failure mode, irrespective of the stiffness properties of the superstructure and constraints imposed at the foundation level. By exploiting this observation, the paper aims at presenting a flexible design methodology that allows the engineer to orient the seismic performance of the soil-foundation-superstructure system toward a predefined cost-effective failure mode, choosing between failure of the foundation, or failure of the above-ground structure, or a combination of both of them.*

1 INTRODUCTION

The cost-effective earthquake design of structures, requires the role of the nonlinear *soil–foundation–structure interaction* (*SFSI*) on the final performance to be explicitly considered. Thus, for the realistic estimation of maximum and residual displacements of foundation-superstructure systems, which in essence constitutes the core of performance-based design philosophy, all sources of nonlinearities should be taken into account; namely nonlinearities developed above and below ground level. In fact, there is a growing awareness among the geotechnical and structural engineering communities towards incorporating the effects of soil compliance into advanced static and dynamic response analysis techniques (e.g. [1]-[6]). Perhaps surprisingly, the field of seismic design of caisson foundations has received little attention (e.g. [7]-[14]).

Simplistic approaches, usually employed in practice, and refer to (a) the separation between structural and geotechnical design, and (b) the modeling of foundation elements, cannot reproduce many essential features of the actual foundation behaviour. It is to this end that the present paper is directed. By means of a series of numerical analyses in 3-D, the response of deeply embedded foundations supporting a single-degree-of-freedom system, which can be representative of a broad range of superstructures (e.g. bridges, wind turbines, etc), is investigated, with due consideration to nonlinearities developed below (soil, caisson-soil interface) and above ground (superstructure). From the analysis, a closed-form expression for the "actual" monotonic load path in *M-Q* space is developed, and a methodology for the preliminary seismic response evaluation, in capacity terms, of deeply embedded (caisson) foundations is proposed.

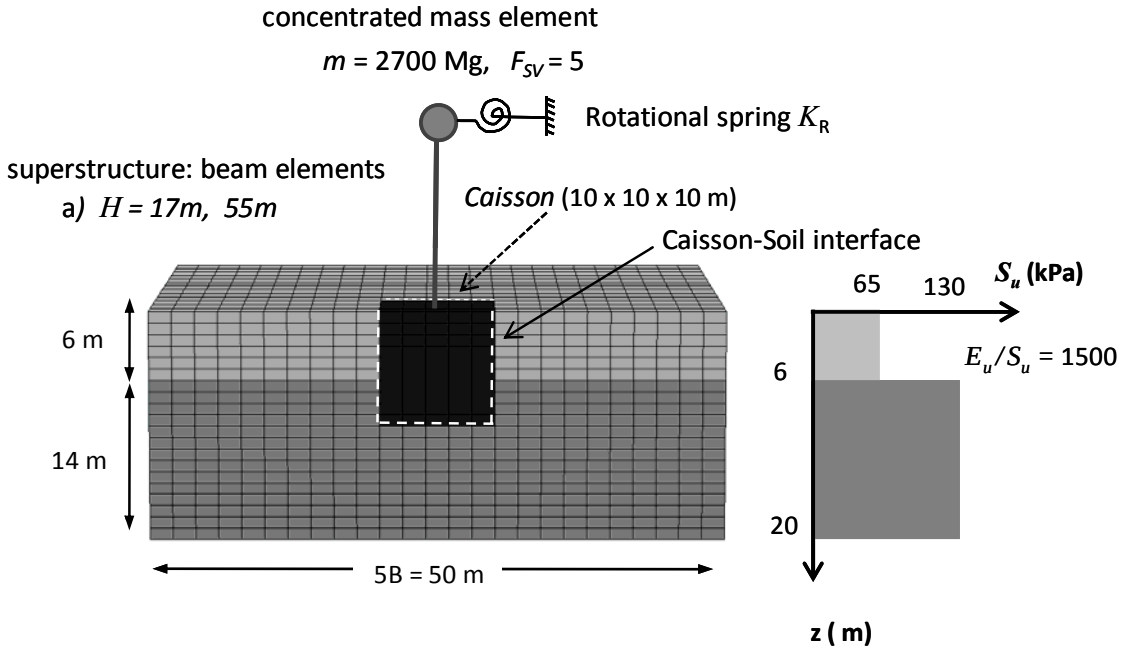

Figure 1. The finite element model

2 PROBLEM DEFINITION

The studied problem is portrayed in Fig. 1. It involves a SDOF system supported by a cubic caisson of side D = 10 m in a 20 m thick 2-layer cohesive soil stratum. The caisson is modeled as a rigid body, with loads and displacements relating to a single load reference point

(LRP), as shown in Fig 2. Two different heights of the superstructure are considered, to represent two different loading conditions with respect to moment loading on the foundation, are used; namely H = 17 m and 55 m. The mass of the system, m, is given the value of 2700 Mg, corresponding to a static factor of safety of FS_V = 5 [11]. The kinematic constraints imposed by the superstructure are simulated by a rotational spring attached at the mass level.

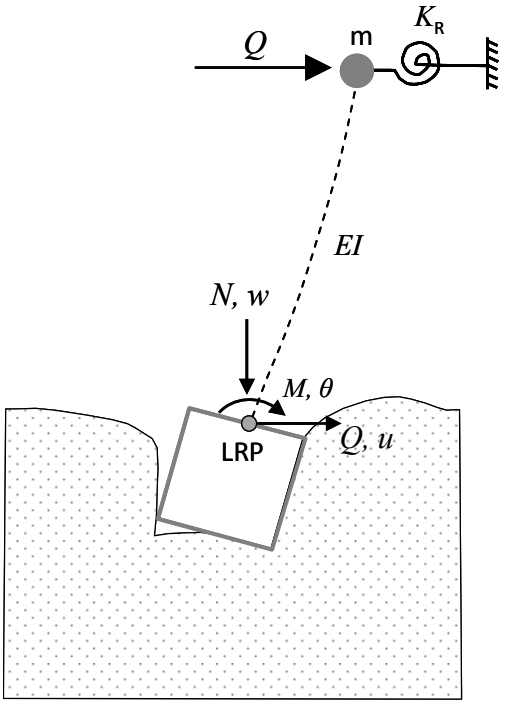

Figure 2. Sketch of the studied problem: A deeply embedded rigid foundation supporting an SDOF superstructure. The kinematic constraints imposed by the superstructure are simulated by a rotational spring attached at the mass level

2.1 Numerical Modeling

The problem is analyzed with use of the finite element code ABAQUS. Both caisson and soil are modeled with 3D 8-noded brick elements, assuming elastic behavior for the former and elasto-plastic for the latter. Fig. 1 shows a half caisson cut through one of the orthogonal planes of symmetry. The size of the finite element mesh is 5B x 5B x 2B carefully weighing the effect of boundaries on the caisson's response and the computational time. Zero-displacement boundary conditions prevent the out of-plane deformation at the vertical sides of the model, while the base is fixed in all three coordinate directions. The caisson is connected to the soil with special contact surfaces, allowing for realistic simulation of the possible detachment and sliding at the soil–caisson interfaces.

The caisson material is modeled as isotropic linear elastic, with a unit weight of γ = 25 kN/m^3, a Young's modulus of E_c = 3 x 10^8 kPa and a Poisson's ratio of v_c = 0.15. However, to ensure rigid body motion appropriate kinematic constraints have been applied between the top central node and all the peripheral nodes of the caisson. The pier columns are modeled with 3-D Timoshenko beam elements, with elasticity modulus E_c = 3 x 10^8 kPa and v_c = 0.15. The stiffness of the rotational spring, K_R, was appropriately modified so that the stiffness ratio:

$$K_{ratio} = \frac{K_R}{\left(\frac{4EI_c}{H}\right)} \tag{1}$$

where ($4EI_c/H$) is the flexural stiffness of the column, yields the following values: $K_{ratio} = 0.1$, 0.25, 0.5, 1.0, for every case examined, covering a wide range of superstructure conditions. Moreover, the case of $K_{ratio} = 0$ (inactive rotational spring) is also provided, for reference.

2.2 Constitutive Models

Soil behavior is described by an elasto-plastic constitutive model [15], which is a reformulation of that originally developed by Armstrong and Frederick [16]. The model is available in the material library of ABAQUS. It uses the Von Mises failure criterion along with a nonlinear combined kinematic—isotropic hardening law and an associated plastic flow rule. The clayey soils are saturated responding in undrained fashion with shear strength S_u = 65 kPa at the upper 6 m, S_u = 130 kPa at the lower 14 m and a constant stiffness to strength ratio E_u / S_u = 1500. The unit weight of the soil materials is taken γ = 20 kN/m^3. To approximate the constant volume response under undrained conditions, a Poisson's ratio of $\nu \approx 0.5$ (= 0.475 to avoid numerical instabilities) was assumed.

Nonlinear response is introduced for the superstructure by means of a bi-linear moment-rotation law (Fig 3) for the rotational spring and a bi-linear moment-curvature law for the pier (beam), The values of the bi-linear laws are deliberately pre-defined, so that structural failure precedes bearing capacity failure of the foundation.

2.3 Failure Envelope

At first, a series of finite element (FE) static pushover-type of analyses are carried out to derive the bearing strength surface of the caisson–soil system in *M-Q* space [10], [17], [18]. Firstly, the soil undergoes geostatic loading and then a part of the soil is replaced by the foundation, on which a vertical load is applied till the specified value of the factor of safety (FS_V = 5) is reached. Afterwards, the vertical load is kept constant and a combination of horizontal force Q and overturning moment M is applied at the head of the caisson until failure. By a series of force-controlled analyses the strength surface is ultimately determined. The surface is presented normalized with respect to the pure moment capacity M_u (with no horizontal loading) and the pure horizontal capacity Q_u (no moment loading) of the foundation (Q_u = 44 MN, and M_u = 430 MNm for the studied cases).

It has been shown in [10], [18], that an ellipsoid of the general form:

$$f = \left(\frac{Q}{Q_u}\right)^{n_1} + \left(\frac{M}{M_u}\right)^{n_2} + n_3\left(\frac{Q}{Q_u}\right)\left(\frac{M}{M_u}\right) - 1 = 0 \tag{2}$$

can adequately fit the numerical results in the normalized *M-Q* space at a particular vertical load level (N). The coefficients n_1, n_2 affect the skewness with respect to the axis of symmetry, while n_3 controls the size (expansion-contraction) of the surface. They are functions of the embedment ratio D/B, vertical load and interface conditions [19]. For fully bonded interface conditions $n_1 = n_2 = 2$ (zero skewness), while n_3, for any practical reason, depends only on the embedment ratio ([10], [18]):

$$n_3 = 1.84 - 0.21\left(\frac{D}{B}\right)^{-1.98} \tag{3}$$

Apparently, for nonlinear interface conditions (gapping and slippage) the coefficients are described by more complex functions, as suggested in [19].

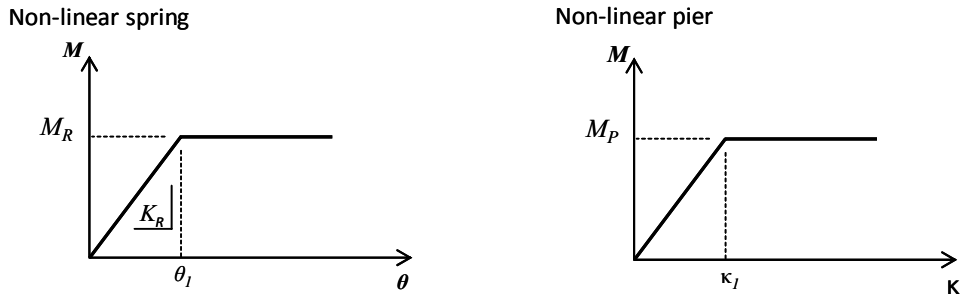

Figure 3. Bi-linear moment-rotation and moment-curvature laws used to model the spring and the pier, respectively.

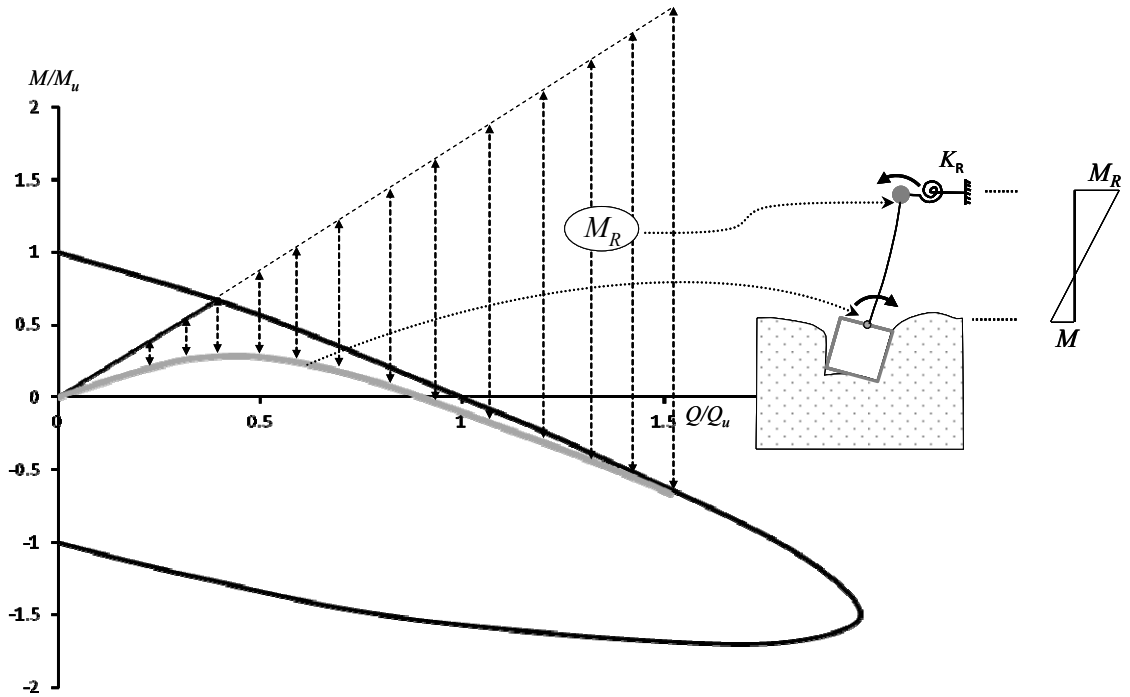

Figure 4. Geometric representation of the moment developed at the head of the caisson (grey solid line) and the rotational spring, M_R , assuming linear response.

3 ANALYSIS RESULTS

Having determined the bearing strength surface of the caisson, the whole soil-foundation-superstructure system is then subjected to lateral loading at the mass level, monotonically increasing until system failure. The analysis terminates either due to bearing capacity failure of the foundation or due to failure of the superstructure. Throughout the analysis, the load path on the foundation is being constantly tracked in *M*-*Q* space.

The presentation of the methodology and the results precedes a graphical illustration (Fig 4) that serves to elucidate the contribution of each of the load-carrying mechanisms within the foundation-superstructure system. Yet, the emphasis is given to the response of the foundation.

The caisson and the pier base are subjected to moment loading that is represented by the load path. The moment that develops at the rotational spring (M_R), however, is given by the

vertical distance between the load path and the (extended) line corresponding to the respective (for that specific pier height) cantilever beam (K_R = 0). It should be noted that Fig. 4 portrays an ideal case, in which the beam and the rotational spring respond elastically, and they are therefore capable of carrying substantial loading.

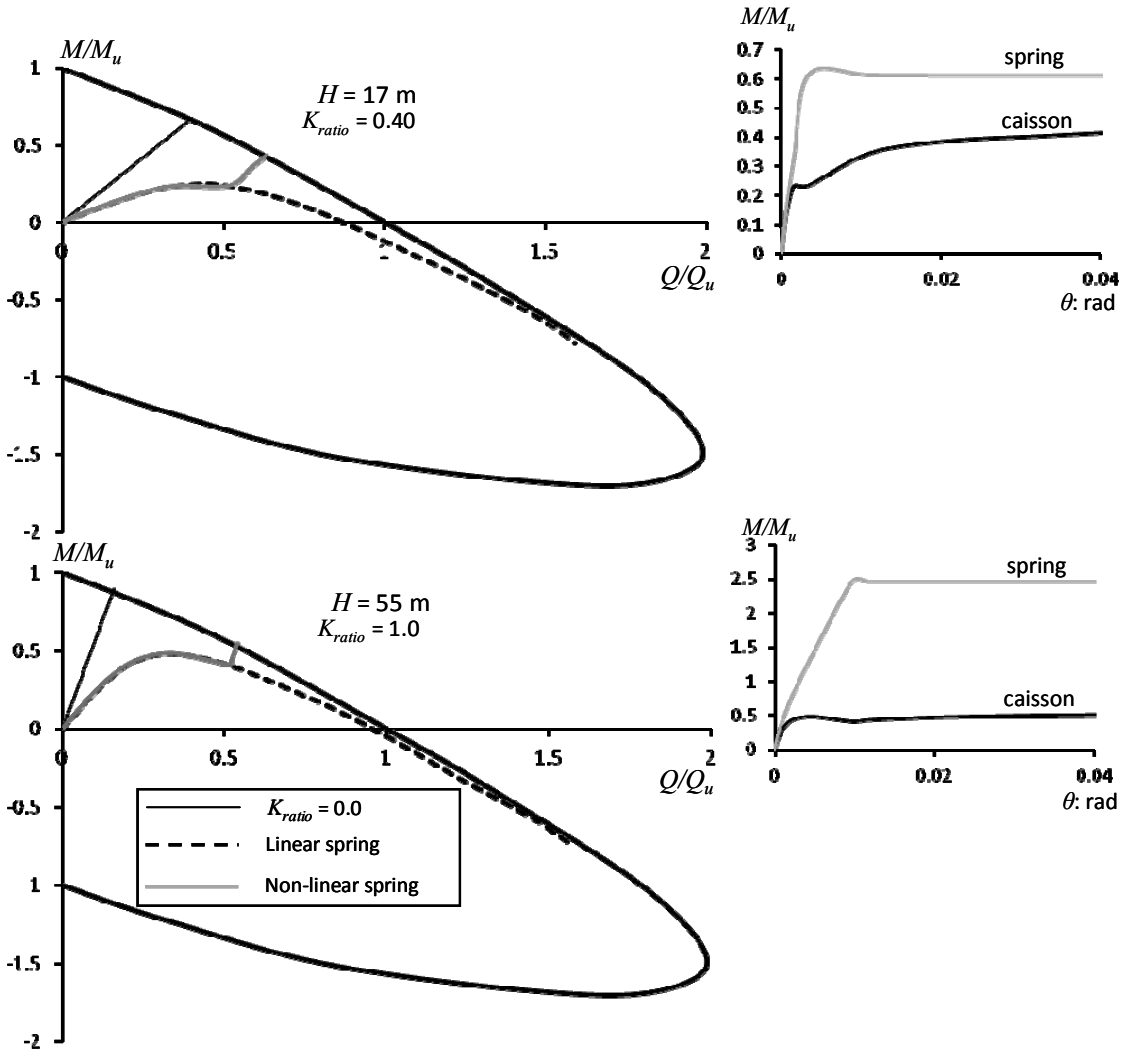

Figure 5. FE results for the load path at the caisson foundation, assuming a linear elastic pier and a nonlinear or linear rotational spring. The corresponding evolution of the moment developed at the top of the caisson (solid black line) and at the rotational spring (solid grey line) with respect to the caisson's rotation, are plotted alongside.

To begin with, we consider a nonlinear rotational spring attached to the top of an elastic pier column. Three characteristic cases are examined, the properties of which, along with the predefined values of the bilinear moment-rotation model for the spring, are given in Table 1.

H : m	M_R : MNm	K_{ratio}	θ_1 : rad
17	276	0.40	0.0023
55	1070	1.0	0.0035

Table 1. Predefined bilinear moment-rotation values for the rotational spring

The results are shown in Fig 5. For reference, each characteristic response is accompanied with the respective ones considering (a) cantilever beam (K_R = 0), and (b) a linear rotational spring. Moreover, the evolution of the normalized moment loading on the foundation (solid black line) and of the rotational spring (solid grey line) with respect to the caisson rotation, are given alongside. For clarity reasons, the negative (in sign) moment developed at the rotational spring is plotted in absolute values.

The computed response can be interpreted as follows: as long as the spring is loaded within its elastic regime, the loading on the foundation follows the respective nonlinear path (dashed line). However, when the moment capacity of the spring (M_R) is reached, denoting the formation of a plastic hinge, the spring cannot sustain any further increase in moment loading. The additional moment is now imposed onto the foundation as positive (in sign) loading, and the system exhibits the response of a caisson carrying a cantilever beam; the load path is tracked parallel to the respective one of a cantilever with height H, and continues until bearing capacity failure of the foundation occurs.

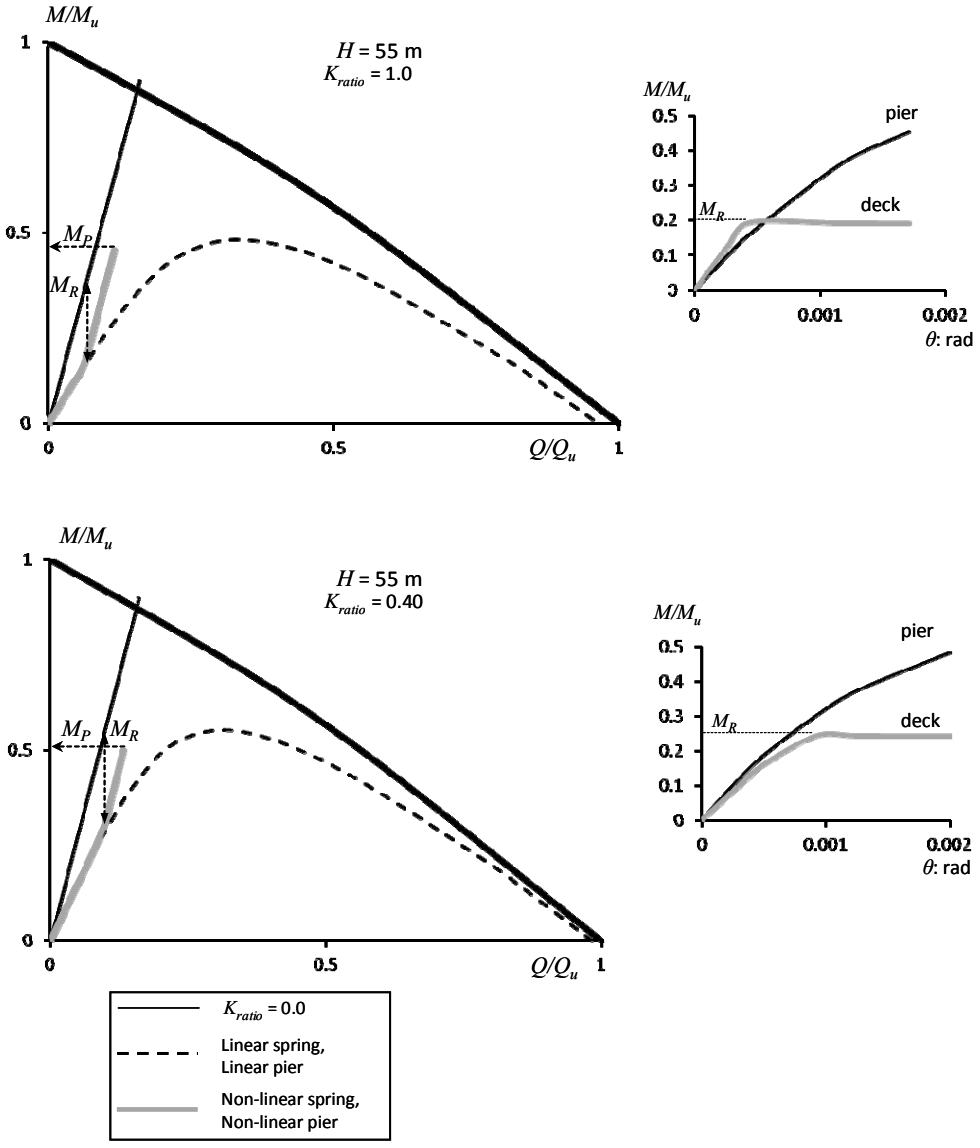

Figure 6. FE results for the load path at the caisson foundation, assuming (a) linear, and (b) nonlinear rotational spring and pier. The corresponding evolution of the moment developed at the top of the caisson (solid black line) and at the rotational spring (solid grey line) with respect to the caisson's rotation, are plotted alongside.

The response is now examined accounting for nonlinear behaviour of both the pier and the rotational spring. Two characteristic cases are considered: a pier height of H = 55 m, kinematically restrained at the mass level by a rotational spring that yields a stiffness ratio of (a) K_{ratio} = 0.40, and (b) K_{ratio} = 1.0. The values for the bi-linear models (as schematically shown in Fig 5) are given in Table 2. Given that the determination of shear strength, and especially of shear deformation characteristics of (e.g. reinforced concrete) structures are still controversial issues [20], the interplay between shear and flexure in the inelastic regime is not taken into account and the controlled mode of failure of the piers is assumed to be flexure-dominated.

H : m	M_P:MNm	κ_1 : rad/m	κ_2 : rad/m	M_R:MNm	K_{ratio}	θ_1 : rad
55	215	0.0000544	0.000055	107	0.4	0.00089
55	195	0.0000493	0.000051	85	1.0	0.00028

Table 2. Predefined bilinear moment-curvature and moment-rotation values for the pier column and rotational spring, respectively

The results, provided in Fig 6, highlight that contrary to the "ductile" progressive failure of the superstructure-foundation system observed following the yielding of the rotational spring, column yielding leads in an abrupt system failure. This "brittle-type" system response is further illustrated from the graphs of the normalized moment loading at the pier base (solid black line) and the rotational spring (solid grey line) with respect to the caisson rotation, which are plotted alongside the load paths.

In summary of the above, Fig 7 schematically represents the nonlinear SFSI effects, and identifies the possible failure modes of the system; point 1 signifies pier column failure; point 2 corresponds to yielding of the rotational spring, followed by a ductile foundation response; point 3 indicates bearing capacity failure of the foundation.

4 DESIGN METHODOLOGY

Based on the analysis presented in the preceding section, an analytical representation of the load path in M-Q space is attempted. Hence, a generalized expression of the following form is considered:

$$\frac{M}{M_u} = \gamma \left[(1+\alpha) \left(1 - e^{-\beta \frac{Q}{Q_u}} \right) - \alpha \frac{Q}{Q_u} \right] \tag{4}$$

where the coefficients α, β and γ control the shape of the load path, and depend on: the properties of the beam (H, I_c), the rotational stiffness of the spring (K_R), and the pure uniaxial capacities of the foundation (Q_u, M_u), which incorporate the effects of soil conditions and foundation's geometry. The determination of the three unknown coefficients requires the consideration of appropriate conditions. These conditions are identified from Fig 8, where the collection of the load paths for all examined cases is plotted, and detailed in the same figure. More specifically:

1. Point ***C***, is the point on the failure envelope associated with the "inverted" pendulum failure mechanism, on which the load paths terminate. Point ***C*** can be considered as an attractor of the caisson response at failure, irrespective of the stiffness properties and constraints at the superstructure system. Its coordinates can be derived from the following conditions:

Point ***C*** lies on the failure envelope. Therefore, satisfaction of the respective equation ($f = 0$) for caisson foundations [10], [18], [19] requires that:

$$f = \left(\frac{Q}{Q_u}\bigg|_C \right)^{n_1} + \left(\frac{M}{M_u}\bigg|_C \right)^{n_2} + n_3 \left(\frac{Q}{Q_u}\bigg|_C \right)\left(\frac{M}{M_u}\bigg|_C \right) - 1 = 0 \tag{5}$$

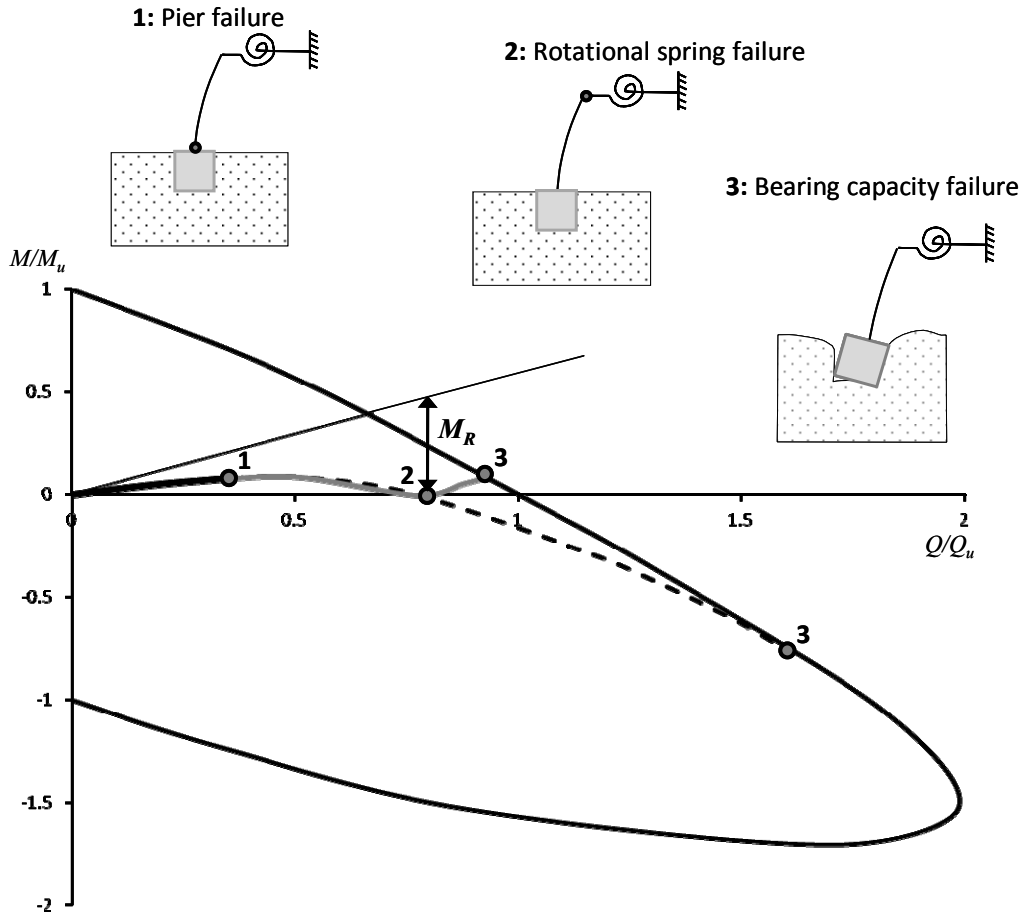

Figure 7. Schematic illustration of all possible failure modes of a caisson supported superstructure accounting for nonlinearities above and below ground level.

Invoking normality conditions for the incremental plastic deformation of the caisson (with respect to its head) at failure, as has been conjectured by several researchers (e.g. [10], for deeply embedded foundations, D/B > 1 and [21], [22] for shallow embedded foundations, D/B < 1), the ratio of the plastic displacement increments can be obtained by differentiating Eq 5 with respect to Q and M, respectively. However, the incremental plastic displacement to rotation ratio for rigid caisson foundations at failure is by definition equal to the depth of the rotation pole, z_p , which in turn is equal to the embedment depth of the caisson ($z_p = D$) when the "inverted" pendulum failure mechanism is manifested. This results in an additional equation that must be satisfied by the coordinates of point ***C***:

$$\frac{\delta u_p}{\delta \vartheta_p} = \frac{\dfrac{\partial f}{\partial Q}}{\dfrac{\partial f}{\partial M}} = \frac{\dfrac{M\, n_3}{M_u\, Q_u} + \dfrac{n_1\, \mathrm{sign} Q \left(\dfrac{|Q|}{|Q_u|}\right)^{n_1-1}}{|Q_u|}}{\dfrac{Q\, n_3}{M_u\, Q_u} + \dfrac{n_2\, \mathrm{sign} M \left(\dfrac{|M|}{|M_u|}\right)^{n_2-1}}{|M_u|}} = D \tag{6}$$

in which δu_p and $\delta \vartheta_p$ are the incremental plastic displacement and rotation at failure, respectively, with respect to the caisson head. Eqs 5 and 6 form a nonlinear algebraic system, from which the coordinates of point ***C*** can be derived.

Substituting the solution of the aforementioned system ($\left.\frac{Q}{Q_u}\right|_C$, $\left.\frac{M}{M_u}\right|_C$) into Eq 4, gives the equation for the first condition:

$$\left.\frac{Q}{Q_u}\right|_C = \gamma \left[(1+\alpha)\left(1 - e^{-\beta\frac{\pi}{2}}\right) - \alpha \left.\frac{M}{M_u}\right|_C \right] \tag{7}$$

2. Point ***A***, that corresponds to the slope of the tangent to the load path at the initial stages of loading. The tangent represents the load path when considering a cantilever beam of initial effective height H_{eff}. Given that $M = H_{eff}\, Q$, the equation of the tangent in the normalized $M/M_u - Q/Q_u$ space can be rewritten as:

$$\frac{M}{M_u} = \left(H_{eff} \frac{Q_u}{M_u} \right) \frac{Q}{Q_u} \tag{8}$$

where $H_{eff} \dfrac{Q_u}{M_u}$ is the respective slope. By differentiating Eq.7 with respect to Q/Q_u, one obtains:

$$\frac{\partial\left(\dfrac{M}{M_u}\right)}{\partial\left(\dfrac{Q}{Q_u}\right)} = \gamma \left[(1+\alpha)\left(1 + \beta e^{-\beta\frac{Q}{Q_u}}\right) - \alpha \right] \tag{9}$$

At the region of initial lateral loading, where $Q/Q_u \to 0$, the slope of the tangent can be substituted into Eq 9, resulting in the following condition:

$$H_{eff} \frac{Q_u}{M_u} = \gamma \left[(1+\alpha)(1+\beta) - \alpha \right] \tag{10}$$

The effective height can be estimated by the following analytical expression:

$$H_{eff} = \frac{2EI_c K_R K_{HM} - 2EI_c K_{HM}^2 H - K_R K_{HM}^2 H^2 + K_R K_H K_M H^2 + 2EI_c K_H K_M H}{2\left(EI_c K_R K_H - K_R K_{HM}^2 H - EI_c K_{HM}^2 + EI_c K_H K_M + K_R K_H K_M H\right)} \tag{11}$$

in which K_H, K_M , K_{HM} and K_{MH} are the swaying, rocking and cross-swaying-rocking initial (elastic) stiffnesses, respectively, of the caisson.

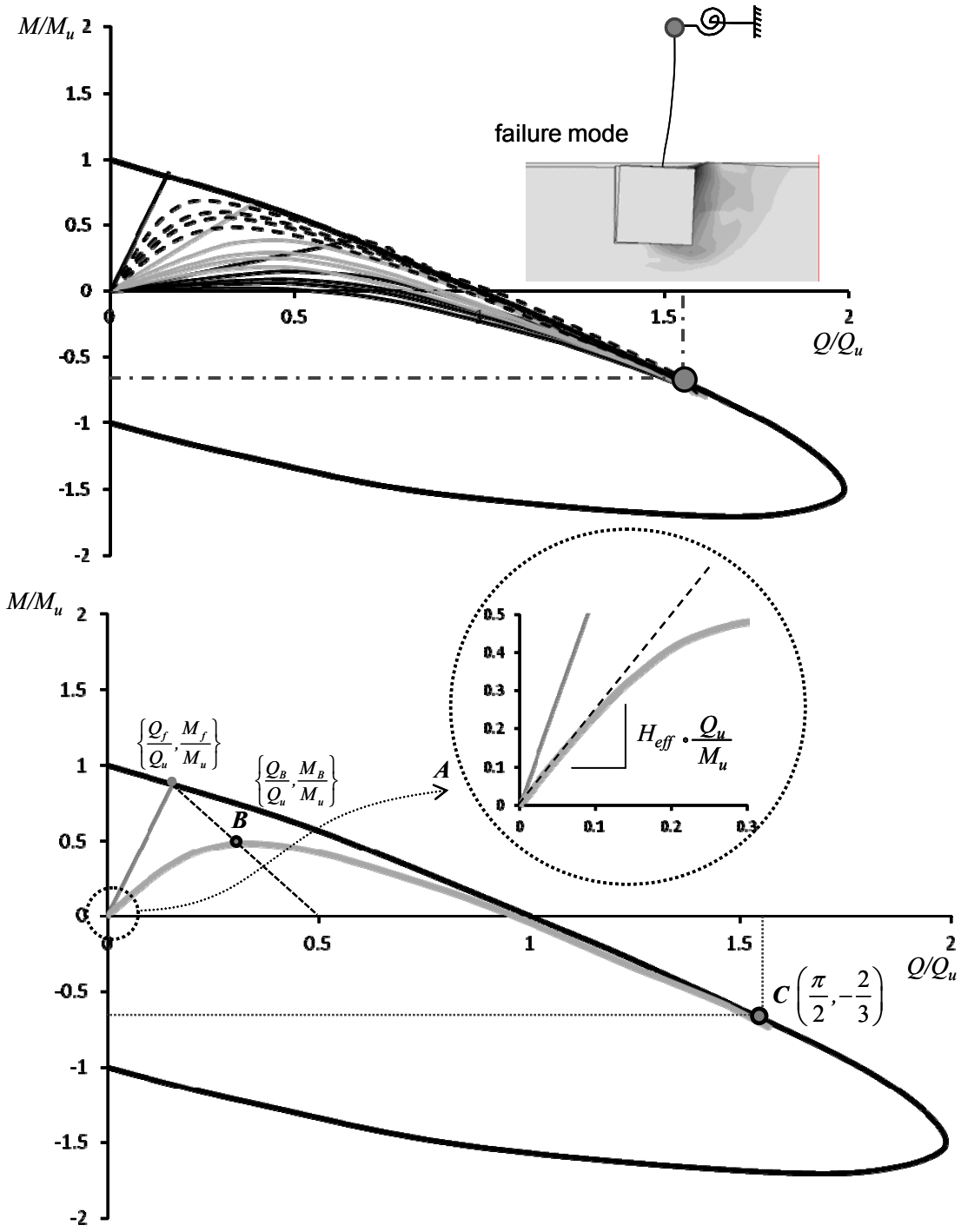

Figure 8. (top) Calculated load paths for all cases examined in this study assuming linear superstructure. All paths are associated with a failure mechanism of the inverted pendulum type (as shown by the corresponding snapshot at failure of the deformed FE mesh. (Bottom) Graphical representation of the three conditions applied for the extraction of a closed-form expression for the load path. The particular coordinates at point ***C*** belong to the failure envelope of caisson foundations with D/B = 1.

3. Point ***B***, which marks the maximum positive (in sign) value of M/M_u, with coordinates $\left\{\frac{Q_B}{Q_u},\frac{M_B}{M_u}\right\}$. Furthermore, point ***B*** is also the point of intersection between (a) the nonlinear load path, and (b) the (dashed) line that connects the point where the linear load path of the respective cantilever (K_R = 0) meets the failure envelope $\left\{\frac{Q_f}{Q_u},\frac{M_f}{M_u}\right\}$, and the abscissa at $\{0.5,\ 0\}$. Hence, and after some algebra, the following expression for the third condition is derived:

$$\frac{1}{\beta}ln\left(\frac{\beta(1+\alpha)}{\alpha}\right)\left(\frac{-2HQ_u}{HQ_u-M_u}-\alpha\gamma\right)-(\gamma+\alpha\gamma)\left(\frac{\alpha}{\beta(1+\alpha)}+1\right)=\frac{HQ_u}{HQ_u-M_u} \tag{12}$$

Eqs 7, 10 and 12 constitute a system of nonlinear algebraic equations, the solution of which yields the parameters α, β and γ, and thus the equation of the load path from the beginning of loading until complete failure of the caisson.

With the load path known, or alternatively, with known the moment and shear force at the head of the caisson (or at the base of the pier), the moment of the rotational spring is calculated by subtracting the response with respect to the caisson head from the hypothetic one of the respective cantilever:

$$M_R = HQ - M \tag{13}$$

Based on the aforementioned methodology, the dimensions of the caisson (width B and depth D), can be effectively estimated targeting either to bearing capacity (foundation) failure, or to structural (pier) failure.

5 CONCLUSION

3D finite element analyses were carried out for the lateral response of deeply embedded (caisson) foundations supporting kinematically constrained single-degree-of-freedom systems, via a rotational spring attached to the mass. The results are used for developing a versatile design methodology allowing for the seismic performance of the soil-foundation-superstructure system to be directed toward a predefined cost-effective failure mode, choosing between failure of the foundation, or failure of the above-ground structure or a combination of both of them.

ACKNOWLEDGEMENTS

Nikos Gerolymos acknowledges the financial support from the European Union (European Social Fund-ESF) and Greek national funds through the Operational Program "Education and Lifelong Learning" of the National Strategic Reference Framework (NRSF)-Research Funding Program: THALES. Investing in Knowledge society through the European Social Fund.

REFERENCES

[1] Bienen B, Cassidy MJ. Advances in the three-dimensional fluid-structure-soil interaction analysis of offshore jack-up structures. *Marine Structures*, 19 (2-3), 110-140, 2006.

[2] Cassidy MJ, Eatock TR, Houlsby GT. Analysis of jack-up units using a Constrained New Wave methodology. *Applied Ocean Research*, 23, 221-234, 2001.

[3] Cassidy MJ, Taylor PH, Eatock TR, Houlsby GT. Evaluation of long-term extreme response statistics of jack-up platforms. *Ocean Engineering*, 29(13), 1603-1631, 2002.

[4] Cassidy MJ, Byrne BW, Randolph MF. A comparison of the combined load behaviour of spudcan and caisson foundations on soft normally consolidated clay. *Géotechnique*, 54(2), 91-106, 2004.

[5] Martin CM, Houlsby GT. Jackup units on clay: structural analysis with realistic modelling of spudcan behaviour. In: *Proc. 31st Offshore Technology Conf.*, Houston, 1999, OTC 10996.

[6] Vlahos G, Cassidy M.J, Martin CM. Numerical simulation of pushover tests on a model jack-up platform on clay. *Géotechnique*, 61 (11), 947-960, 2011.

[7] Williams MS, Thompson RSG, Houlsby GT. Non-linear dynamic analysis of offshore jack-up units. *Computers and Structures*, 69(2), 171-180, 1998.

[8] Hutchinson TC, Chai YH, Boulanger RW, Idriss IM. Inelastic Seismic Response of Extended Pile-Shaft-Supported Bridge Structures. EERI *Earthquake Spectra*, 20(4), 1057-1080, 2004.

[9] Silva PF, Manzari MT. Nonlinear Pushover Analysis of Bridge Columns Supported on Full-Moment Connection CISS Piles on Clays. EERI *Earthquake Spectra*, 24(3), 751-774, 2008.

[10] Gerolymos N, Zafeirakos A, Souliotis C. Insight to Failure Mechanisms of Caisson Foundations Under Combined Loading: a Macro-Element Approach. In: *Proceedings of the 2nd International Conference on Performance-Based Design in Earthquake Geotechnical Engineering*, 28-30 May, Taormina, Italy, Paper No: 11.10, 2012.

[11] Zafeirakos A, Gerolymos N. On the seismic response of *under*-designed caisson foundations. *Bulletin of Earthquake Engineering*, 11(5), 1337–72, 2013.

[12] Zafeirakos A, Gerolymos N, Drosos V. Incremental dynamic analysis of caisson-pier interaction. *Soil Dynamics and Earthquake Engineering*, 48, 71–88, 2013.

[13] Varun, Assimaki D, Gazetas G. A simplified model for lateral response of large diameter caisson foundations-Linear elastic formulation. *Soil Dynamics and Earthquake Engineering*, 29(2), 268-291, 2009.

[14] Tsigginos C, Gerolymos N, Assimaki D, Gazetas G. Seismic response of bridge pier on rigid caisson foundation in soil stratum. *Earthquake Engineering & Engineering Vibration*, 7(1), 33-44, 2008.

[15] Gerolymos N, Gazetas G. Static and dynamic response of massive caisson foundations with soil and interface nonlinearities–validation and results. Soil Dynamics and Earthquake Engineering, 26(5), 377–94, 2006.

[16] Armstrong PJ, Frederick CO. A mathematical representation of the multiaxial Bauschinger effect. Technical Report RD/B/N 731, Central Electricity Generating Board,

Berkeley, UK, 1966 [Reprint in: Armstrong PJ, Frederick CO. A mathematical representation of the multiaxial Bauschinger effect. *Materials at High Temperatures*, 24(1), 1–26, 2007.

[17] Gourvenec S. Bearing capacity under combined loading - a study of the effect of shear strength heterogeneity. In: *Proceedings of the 9th Australian and New Zealand Conference on Geomechanics*, Auckland, New Zealand, 527-533, 2004.

[18] Karapiperis K, Gerolymos N. Combined loading of caisson foundations in cohesive soil: Finite element versus Winkler modeling. *Computers and Geotechnics*, 56, 100–120, 2014.

[19] Karapiperis K. Insight to the numerical modeling of the lateral response of caisson foundation to static and cyclic loading, *Diploma thesis*, NTUA, 2013.

[20] Mergos PE, Kappos AJ. Seismic damage analysis including inelastic shear–flexure interaction. *Bulletin of Earthquake Engineering*, 8, 27–46, 2010.

[21] Cassidy MJ, Randolph MF, Byrne BW. A plasticity model describing caisson behaviour in clay. *Applied Ocean Research*, 28, 345–358, 2006.

[22] Martin CM, Houlsby GT. Combined loading of spudcan foundations on clay: Numerical modelling. *Géotechnique* , 51(8), 687-699, 2001.